Top Med Chem (2020) 34: 203–224
DOI: 10.1007/7355_2019_84

Published online: 8 February 2020

# The Present and Future of Optical Imaging Technologies in the Clinic: Diagnosis and Therapy


**Evan P. Stater, Magdalena Skubal, Ryo Tamura, and Jan Grimm**

## Contents



**Abstract** Medical techniques based upon optical imaging technologies are important tools in clinical practice. The use of optical imaging in medical diagnosis is well established, and a large array of techniques are in current use, such as white light endoscopy, autofluorescence imaging, and optical coherence tomography. The applications of these techniques are expanding, and newer imaging technologies are becoming available to address problems and limitations associated with existing methods. Beyond diagnostics, optical imaging is increasingly a useful component of interventional medical procedures, such as image-guided surgery. In procedures such as surgical tumor resection, fluorescence imaging can aid surgeons in improving both accuracy and completeness of removal. Relevant to both diagnostic and therapeutic applications, Cerenkov luminescence imaging is a potential clinical technique which relies upon generation of visible-spectrum light by beta particles in a dielectric medium; this method could allow for coupling of a multimodal optical component to existing molecular imaging techniques, such as positron emission tomography, and also provide a means of monitoring distribution of administered clinically relevant radionuclides such as lutetium-177.

E. P. Stater
Weill Cornell Medicine, New York, NY, USA

M. Skubal and R. Tamura
Memorial Sloan Kettering Cancer Center, New York, NY, USA

J. Grimm (✉)
Weill Cornell Medicine, New York, NY, USA

Memorial Sloan Kettering Cancer Center, New York, NY, USA
e-mail: grimmj@mskcc.org

**Keywords** Cerenkov luminescence imaging, Clinical imaging, Diagnostic imaging, Endoscopy, Intraoperative imaging

## 1 Introduction

Optical imaging modalities are a crucial component of medical diagnosis and treatment. They are widely utilized for both diagnostic and interventional procedures. Thanks to the rapid pace of innovation in optical imaging technologies, clinicians have a wider array of imaging tools available than ever before. Furthermore, a number of promising new modalities are approaching clinical viability, for a broad variety of applications. This review will describe the current state of optical-based imaging modalities in diagnosis via endoscopic imaging and in treatment via image-guided surgery. Additionally, Cerenkov luminescence imaging, a promising new technology with many potential medical applications, will be described in detail.

## 2 Diagnostic Endoscopic Imaging

Endoscopy, a classification of medical procedures which utilize an endoscope to examine the endoluminal surfaces of internal body cavities, is a vitally important clinical tool, both for diagnosis and for guidance of interventional procedures such as surgery. Information gleaned from diagnostic endoscopic examinations help clinicians diagnose diseases and guide treatment decisions. Naturally, optical imaging technologies are integral to endoscopic procedures. This review section will discuss the current state and technological horizon of optical imaging modalities in diagnostic medical endoscopy.

**Optical Imaging and Clinical Endoscopy** The current standard of care for most clinical endoscopic imaging is non-fluorescent white light endoscopy (WLE). This optical imaging modality relies upon full-spectrum visible light illumination for visualizing internal anatomy. It can be used both for wide-field imaging and, with magnification, for examination of internal microanatomy. Although WLE is widely used clinically and does not require the administration of contrast agents, it has many shortcomings. Endoscopic diagnosis with WLE relies mainly upon the clinician's subjective ability to recognize macroscopic or microscopic morphological abnormalities in surface mucosa and other superficial structures. Generally, WLE is useful for the detection of conspicuous and superficial abnormalities; indistinct and non-facile abnormalities may escape detection with WLE. Furthermore, WLE detection of lesions is often not sufficient to merit diagnosis; invasive tissue biopsy

samples and subsequent histopathological analysis are frequently required for confirmation. Due to these limitations, newer optical imaging technologies are coming to the forefront to improve both the utility and versatility of endoscopy as a diagnostic technique.

**Visible-Spectrum Modalities** Several visible-spectrum optical imaging technologies have emerged with the aim of improving the accuracy, sensitivity, and specificity of WLE. The most widely used, chromoendoscopy, utilizes the administration of colored dyes as contrast agents to provide differentiating contrast to specific tissues and anatomical structures. A wide variety of application-specific dyes can be used for chromoendoscopic procedures. Administered dyes can be absorptive to specific epithelia or tissue types (e.g., methylene blue with upper gastrointestinal endoscopy for detection of Barrett's esophagus), non-absorptive to highlight extracellular structure and tissue topography (e.g., indigo carmine with colonoscopy for detection of colon polyps), or reactive to detect specific biochemical processes (e.g., phenol red with gastroendoscopy to visualize gastric *Helicobacter pylori* infection). A key advantage of this method is that it does not require the purchase of expensive specialized endoscopes, but rather can be performed with existing WLE equipment. However, it does require patient administration of contrast dyes, which can be unpleasant and invasive, and/or carry the risk of potential side effects. Furthermore, many chromoendoscopic procedures require removal of mucus in the region of interest prior to application of the contrast dyes, increasing the clinical time, complexity, and cost of the procedure.

Narrowband imaging (NBI) is a newer technology based on visible-spectrum light, in which white endoscopic illumination light is filtered into specific wavelengths, typically at 415 nm (blue light) and/or 540 nm (green light). These light bands correspond to the optimal absorptive wavelengths of hemoglobin contained in shallow mucosal blood vessels or deeper basal layer blood vessels, respectively. NBI endoscopy therefore enhances the optical contrast of blood vasculature over conventional WLE without requiring the administration of contrast agents (Fig. 1a). It can be useful for improving visual identification of vascular abnormalities that are associated with disease conditions, such as neoplasia. However, performing NBI endoscopy requires the purchase of NBI-capable endoscope systems.

So-called "digital endoscopy" procedures utilize legacy WLE equipment with the addition of software-based image post-processing to improve the quality of endoscopic images and provide more relevant information to clinicians. Post-processing is flexible and can be applied to conventional WLE, NBI, or chromoendoscopic procedures (Fig. 1b). Software suites available for this purpose include Fuji Intelligent Chromo Endoscopy (FICE) by Fujinon Corporation (Saitama, Japan) and Pentax i-SCAN by HOYA Corporation (Tokyo, Japan.) Usage of these software suites has shown some benefits in certain clinical diagnostic applications, but comparative results have generally been mixed. The i-SCAN suite has been shown to improve diagnosis of esophagitis when coupled with WLE versus WLE alone [6]; however, it also failed to show significant improvement in diagnosis of gastric neoplasia or small adenomatous colon polyps [7, 8]. Similarly, FICE software has

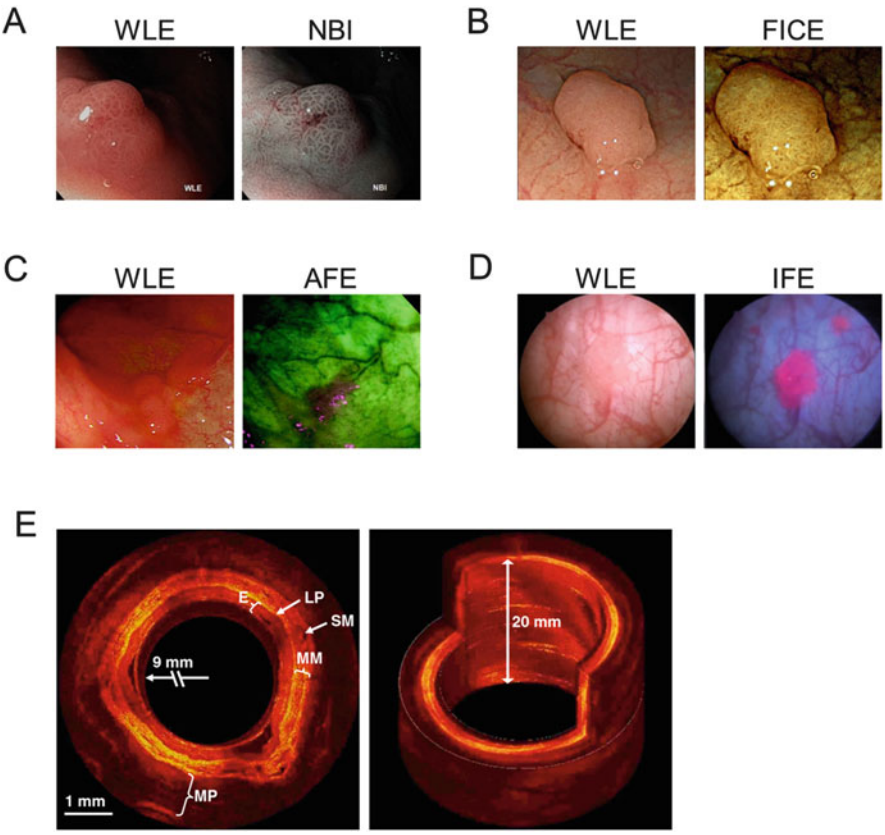


**Fig. 1** (**a–d**) Comparison of endoscopic optical imaging modalities to conventional white light endoscopy (WLE). (**a**) An intestinal dysplasia imaged by WLE and narrowband imaging (NBI) [1]. (**b**) A neoplastic colon polyp imaged by WLE with and without Fuji Intelligent Chromo Endoscopy software (FICE) image post-processing [2]. (**c**) A colon adenoma imaged by WLE and autofluorescence imaging (AFE) [3]. (**d**) A papillary bladder lesion imaged in bladder cystoscopy with hexaminolevulinate by WLE and induced fluorescence endoscopy (IFE) [4]. (**e**) Example of 2D cross-sectional and 3D reconstructed images of a porcine esophagus imaged via optical coherence tomography (OCT), demonstrating micron-scale resolution of subsurface esophageal strata. Muscularis propria (MP), submucosae (SM), muscularis mucosae (MM), lamina propria (LP), and epithelium (E) can be identified [5]. Referenced figure panels have been adapted and reprinted with permission of their respective owners

shown improvement in detection of depressed-type gastric neoplastic lesions [9] but not in detection of adenomatous colon polyps [10].

**Fluorescence Imaging Modalities** Fluorescence imaging is an emerging and promising avenue for the present and future of clinical imaging, including in endoscopic applications. Analogous to WLE in visible-spectrum light imaging, the most widely used form of fluorescence imaging in endoscopic procedures is autofluorescence endoscopy (AFE). AFE endoscopes exploit differences in the

concentrations of naturally occurring fluorophore biomolecules, such as collagen, to generate wide-area images of internal tissues without exogenous contrast agents. Fluorescence excitation is provided by illumination with a high-intensity blue light on the endoscope; emission is visualized (via false color video) with an optical camera configured to capture light at various emission wavelengths. AFE imagery can provide information about abnormalities that may not be easily detectable with WLE, such as differences in tissue density, epithelial thickness, or blood flow rate (Fig. 1c). Though AFE systems can address some of the limitations of standard WLE, they are constrained by many of the same drawbacks. Furthermore, although AFE has been shown to improve detection rates of lesions, it also typically has a higher rate of false positives, such as in detection of early gastric neoplasia [11], necessitating more frequent follow-up biopsy analyses.

Analogous to white light chromoendoscopy, induced fluorescence endoscopy (IFE) relies upon administration of exogenous fluorescent contrast agents and illumination with excitatory wavelength light to visualize specific internal anatomy. IFE can provide enhancement of visual contrast beyond what is possible with WLE, chromoendoscopy, NBI, or AFI. Furthermore, the use of far-red or near-infrared fluorophores with IFE can increase the penetration depth of imaging and enable detection of non-superficial structures and lesions, overcoming a key limitation of other optical endoscopic technologies. However, this newer technology has not yet seen widespread clinical adoption, due mainly to the limited number of fluorescent contrast agents available to clinicians. Frequently used contrast agents in clinical IFE include 5-aminolevulinic acid (5-ALA) and hexaminolevulinate (for cancer detection in upper gastroendoscopy and bladder cystoscopy, respectively) and the near-infrared fluorophore indocyanine green (ICG, for enhanced fluorescent labeling of vasculature) (Fig. 1d). Another near-infrared fluorochrome, methylene blue, is FDA- and EMA-approved as a chromogenic dye; because it is also fluorescent, its use with IFE has been investigated to help surgeons locate and avoid injury to the ureters of colorectal surgery patients [12]. Additionally, IFE holds promise for endoscopic visualization of targeted molecular probes; however, this application has not yet been exploited clinically, due to the lack of targeted fluorescent contrast agents with regulatory approval.

Previously described visible-spectrum imaging modalities are applicable to either wide-area imaging (e.g., during open or laparoscopic surgery) or magnification endoscopy. However, with respect to fluorescence imaging, confocal laser endomicroscopy (CLEM) is the preeminent technology for fluorescent endoscopic examination under magnification. CLEM combines blue laser fluorescence imaging with intravital confocal microscopy, enabling live confocal plane imaging of endoluminar microanatomy at cellular or subcellular resolutions. This enables superior image quality, increased penetration depth, and improved anatomical differentiation when compared to conventional magnification endoscopy. The development of clinical CLEM technology confers two primary benefits to endoscopic diagnosis: first, in some instances, it may permit completely optical percutaneous biopsy of patients, negating the need for potentially traumatic tissue sample collection and outside histopathological analyses; second, in cases where traditional tissue biopsies

are still required, it can enable more accurate identification of relevant biopsy sites. A variety of contrast agents are used in CLEM, though all are currently used off-label for this application. Fluorescein is administered intravenously to provide fluorescent contrast to blood vasculature. Other contrast agents can be applied topically at the imaging site, which may or may not require prior removal of mucin from the surface. Topical imaging agents can include fluorescent stains to highlight intracellular regions and lamina propria (fluorescein sodium) or cell nuclei (cresyl violet or acriflavine). Additional fluorescent contrast agents with longer-wavelength excitation, such as methylene blue, have been demonstrated in preclinical research and could be used in future clinical work as well; however, currently, only scopes equipped with blue light lasers (488 nm) are approved for clinical use. The microscopic field of view of CLEM necessitates wide-area image-guided placement of the CLEM probe prior to image acquisition. Existing CLEM endoscopes usually rely on simultaneous wide-area WLE for correct placement of the microscopic probe at the lesion of interest. Therefore, the CLEM examination site selection is subject to the same limitations inherent to macroscopic WLE. However, other probe guidance methods have been used with CLEM, such as ultrasonography or X-ray fluoroscopy [13, 14].

**Near-Infrared Imaging Modalities** Beyond fluorescence imaging in the clinic, a new technique, optical coherence tomography (OCT), utilizes interferometry with near-infrared (NIR) light backscattering to construct a high-resolution image of three-dimensional tissues from a series of two-dimensional tomographic cross-sectional images. From an application point of view, OCT is similar in function to high-frequency ultrasonography; however, OCT relies on light rather than sound for generation of an image. Furthermore, the emitted near-infrared light is able to traverse air-filled spaces; unlike HF ultrasonography, it does not require direct probe contact (nor a water interface) with the tissue areas of interest. This makes it a useful imaging modality for mapping the surface and subsurface topology of large or expansive endoluminal cavities and therefore highly suited for endoscopic imaging. OCT scans can provide information on cutaneous and subcutaneous endoluminal surface density and morphology, enabling rapid wide-area identification of subsurface abnormalities. OCT endoscopes provide excellent spatial resolution, with sub-20 μm resolutions possible. OCT systems also provide temporal resolution by scanning multiple times per second, thus allowing acquisition and observation of images in real time. The primary benefit of OCT to clinical endoscopy comes in the ability to rapidly map the volumetric microstructure of large and complex endoluminal cavity surfaces (Fig. 1e). Though NIR provides improved light penetration into tissue compared to shorter wavelengths, the depth of OCT scanning is limited to a few millimeters due to excessive light scattering at greater depths. Endoscopic OCT has been clinically approved for upper GI endoscopic procedures and for intravascular endoscopy. It is also being evaluated for a variety of new indications, including diagnosis of urothelial carcinoma in the bladder [15], and imaging of bronchial airway remodeling in patients with chronic obstructive pulmonary disease [16]. A compact OCT endoscope housed within a small,

self-contained capsule-shaped module has been developed for esophageal OCT; the "capsule" is swallowed by a fully conscious patient and then recovered via a narrow tethering fiber. This development raises the possibility of esophageal endoscopy without the need for sedation, which is a significant barrier to early screening of Barrett's esophagus [17].

**Multimodal Imaging** Despite advances in imaging technology, all endoscopic imaging modalities are constrained by inherent physical or technical limitations which limit clinical usefulness. To overcome this, different imaging modalities could be combined together into a single endoscopic procedure, with the ultimate goal of mitigating the shortcomings in one imaging modality by supplementing it with others that are not subject to the same disadvantages. Aside from the use of wide-field WLE, which is routinely used in conjunction with other endoscopic modalities (e.g., to guide magnification endoscopy techniques such as CLEM), multimodal endoscopic imaging is mostly at the investigative stage. Several novel applications have been demonstrated in clinical pilot studies; for example, a trimodal endoscope was devised to combine WLE, NBI, and AFI to reduce the high false-positive rate associated with AFI colonoscopy in screening for colorectal adenomas and for gastric neoplasia [11, 18]; in another study, OCT was combined with WLE and IFE cystoscopy (with hexaminolevulinate) to reduce false positives in the diagnosis of urothelial carcinoma [15].

**Preclinical Modality Pipeline** A number of promising new optical imaging technologies are being evaluated for endoscopic applications.

*Raman spectroscopy*, an imaging technique which relies upon inelastic scattering of laser light to detect differences in vibrational or rotational molecular states, has been investigated for in vivo imaging systems, including endoscopy. Raman spectroscopy is particularly notable for its chemical specificity, which is useful for measuring biochemical states and changes in biological tissue. It can be combined with far-red or near-infrared light sources for deep tissue penetration. Though promising, Raman spectroscopic endoscopy and other Raman-based imaging methods thus far have faced technical obstacles, primarily due to the low intensity of inelastic light scattering signatures, which limit the accuracy and speed of image acquisition compared to existing clinical modalities. A variety of innovative Raman-based imaging technologies have been developed to overcome these limitations, such as selective-sampling Raman spectroscopy, coherent anti-Stokes Raman spectroscopy, surface-enhanced Raman spectroscopy, and spatially offset Raman spectroscopy. Endoscopic Raman spectroscopy has been evaluated in patient feasibility studies for a variety of applications, including colonoscopic identification of precancerous adenomatous polyps, endoscopic diagnosis of gastric dysplasia, and detection of nasopharyngeal cancers [19–21].

Cerenkov luminescence (CL), light emissions caused by the transit of charged particle radiation through a dielectric medium at greater than the speed of light, has been evaluated for medical imaging purposes. The resultant technology, called *Cerenkov luminescence imaging* (CLI), utilizes Cerenkov light generated by the decay of an injected β particle-emitting isotope, which are typically used to provide

radiocontrast in positron emission tomography (PET) scans or for targeted radiotherapy. CLI is adaptable to endoscopy for selected applications and could be useful for optical detection of radiotracers via an endoscope. A prototype CLI endoscope has been demonstrated in animal studies using conventional endoscopic equipment coupled with the PET radiotracer $^{18}$F-fluorodeoxyglucose [22]. Further medical applications of CLI are discussed at length in the latter section of this review.

Incident light that is reflected by tissues is modified in numerous ways by the physical and biochemical properties of that tissue, which manifests in changes to absorbance via intensities of specific wavelengths, variation in angular trajectories, alteration of light polarity, etc. *Reflectance spectroscopy* takes advantage of these resultant differences, using advanced analysis to construct quantitative "scattering signatures" of reflected light to reveal morphological and biochemical information about probed tissues without labeling. For endoscopy, reflectance spectroscopy has several promising applications, most notably to detect the oxygenation level of blood. The ratio of oxyhemoglobin to deoxyhemoglobin can be extrapolated by the differential absorbance and reflectance profiles of each compound, providing an endoscopic tool for detection of poorly perfused regions in mucosal tissue. A white light reflectance spectroscopy method has been used to measure via colonoscopy to analyze the success of induced colon polyp ischemia procedures in real time, as well as identification of sites of mesenteric ischemia [23, 24].

*Two-photon endomicroscopy* (TPEM) is yet another emerging technology with potential to be translated into clinical endoscopy. Two-photon imaging utilizes two excitation photons using a femtosecond pulsed beam to produce fluorescent emission by excitation of individual atoms by two simultaneous photons. This method can utilize near-infrared excitation sources for deep tissue penetration. Furthermore, simultaneous absorbance of two photons is an extremely low-probability event outside of the focal point due to insufficient photon density; therefore, emission from outside the focal point is negligible. This permits exclusion of background light outside of the focal plane, but without the pinhole aperture required in confocal microscopy. TPEM is therefore a potentially advantageous alternative to CLEM, with acquisition of deeper images possible. Like CLEM, however, TPEM would require administration of fluorescent contrast agents. Prototype TPEM units have been demonstrated in animal models but thus far have not yet been evaluated in human patients [25, 26]. Clinical TPEM also requires further development and approval of fluorescent contrast agents which are optimized for two-photon excitation.

**Summary** Diagnostic endoscopic procedures are arguably the most commonly used and most diverse application of optical imaging in medicine today. Nearly every modality of optical imaging in current clinical use is represented in the array of endoscopic imaging technologies currently available to physicians. Furthermore, endoscopic procedures also have the largest frontier of technological advancement, with a number of novel advanced optical technologies at or near the clinical translation threshold.

## 3 Optical Imaging in Interventional Procedures

Beyond diagnostic procedures, optical imaging technologies are of increasing importance in current and future interventional medical techniques. For example, in oncology, surgery is the primary treatment modality for most solid tumors. Although optical imaging plays an essential role in cancer diagnosis and preoperative planning, during the surgery, the operating surgeon often depends on visual appearance and manual palpation to differentiate between tumor and normal tissue and to establish a sufficient tumor-free margin. Reliance on white light limits the visual contrast apparent to the surgeon to a narrow dynamic range in the colorimetric spectrum. Thus, limitations in specificity and sensitivity are a critical aspect of oncologic surgeries, and real-time image guidance is highly desirable in the operating room [27–29].

In this review, we explain the concept of optical image-guided surgery in surgical oncology. Image-guided surgery enables surgeons to perform surgery under the guidance of live intraoperative images, wherein surgeons are able to track the resection area on a monitor with reliable real-time feedback on any remaining tumor tissues or other diseased areas, such as ischemia. Because of the delicate nature and time sensitivity of surgery, the imaging time must be short, and image processing must be rapid – essentially in real time, at high temporal resolution and with minimal latency [30]. As a result, surgical procedures are easier to undertake with greater certainty that the critical landmarks are secured. Tumor cells left behind at the edge of the surgical resection area, defined as positive margins, result in increased recurrence and poor prognosis for patients with head and neck cancer, brain cancer, breast cancer, non-small cell lung cancer, colorectal cancer, and urogenital tract cancer [31–38]. Image guidance allows careful identification of primary and microscopic tumors and the complete removal of cancerous tissue [39].

Elevated cellular metabolism, increased expression of growth factor signaling receptors, hypoxia, and increased tumor angiogenesis are common traits that sustain the hyperproliferative potential of tumor cells. These biomarkers specific to cancer cells or the tumor microenvironment potentially allow cancer to be distinguished from normal tissue and could be exploited as potential targets to direct imaging agents [28]. An approach to incorporate biomarker-targeted molecular imaging agents in the imaging procedure improves the tumor-to-background signal ratio needed for fast assessment of lesions [30, 40]. Ease of image acquisition, relatively low-cost imaging devices, high resolution, and real-time applicability of imaging agents for use in optical imaging methods are highly desirable for use in real-time image-guided surgery [30]. However, there are substantial technical issues such as specific tumor labeling, imaging system portability, and patient-like animal models in which to develop the technology, which need to be addressed for image-guided surgery going forward toward clinical use [41].

**Image-Guided Surgery** Fluorescence-guided surgery emerged as a technique using fluorescence to visualize cancer cells to guide intraoperative procedures. Classical fluorescent techniques primarily use probes in the visible light spectrum

in the wavelength range of 400–600 nm. This spectrum region is related to a higher level of nonspecific background light and limited tissue penetration depth [28]. In the early years of this millennium, fluorescent imaging for cancer-specific navigation was successfully used in neurosurgery. Stummer et al. demonstrated that 5-ALA accumulates as fluorescent protoporphyrin IX in malignant gliomas and helps in their precise surgical resection. Complete resection of tumor tissue with maximal preservation of normal surrounding brain tissue significantly improved survival and life quality of glioblastoma patients (Fig. 2a) [45, 46].

To improve imaging depth with minimal interference of light scattering and tissue autofluorescence, optical modalities utilize fluorescent emission light in the NIR wavelengths of 700–900 nm, known as the first near-infrared window (NIR-I). Furthermore, fluorophores emitting in the range of 1,000–1,700 nm, in the second near-infrared window (NIR-II), were developed to enhance imaging quality at increased tissue depth [47, 48]. The NIR spectrum range allows a high ratio of signal to background in biological tissue and in oncologic imaging yields a high tumor-to-background ratio [30, 49]. Clinical applications of NIR fluorescence imaging have been demonstrated in sentinel lymph node (SLN) mapping, tumor imaging, and visualization of vasculature [50].

At present, clinically approved nontargeted contrast agents for image-guided surgery include ICG and methylene blue (Fig. 2b, c). Their fluorescence emission is localized within the NIR-I spectrum [28, 39]. Applications of ICG include induced NIR fluorescence in cancer-related surgery for SLN mapping, intraoperative identification of solid tumors, and angiography during reconstructive surgery [43] ICG-based imaging agents offer significant improvements during SLN mapping in prostate, breast, gastric, rectal, and vulvar cancers [51–55].

An integrated diagnostic approach based on premixing of ICG with $^{99m}$Tc-nanocolloid resulted in an imaging agent that is both radioactive and fluorescent and enables preoperative and intraoperative SLN imaging in laparoscopic lymph node dissection. ICG-$^{99m}$Tc-nanocolloid injected into the prostate allowed the location of the pelvic sentinel lymph SLNs to be established preoperatively by SPECT/CT imaging. During surgery fluorescence was used to visualize previously identified nodes and improve surgical guidance. Correlation between the radioactive and fluorescent signal in the removed lymph nodes showed that ICG-$^{99m}$Tc-nanocolloid in combination with SPECT/CT and a fluorescence laparoscope can facilitate precise dissection of SLNs [51].

One of the greatest challenges for prostate cancer management is lymphatic spread of metastases, giving rise to tumor recurrences. Lymphatic mapping using radioguidance or fluorescence guidance in surgery via an agent targeting prostate-specific membrane antigen (PSMA) constitutes an alternative to traditional pelvic lymph node dissection. Preoperative PET imaging with $^{68}$Ga-PSMA tracers was the most reliable method for identification of lymphatic macrometastases; by comparison, intraoperative lymphatic mapping with ICG-$^{99m}$Tc-nanocolloid via a fluorescence imaging camera combined with a handheld γ-ray probe was shown to be the most reliable for identifying micrometastases [56].

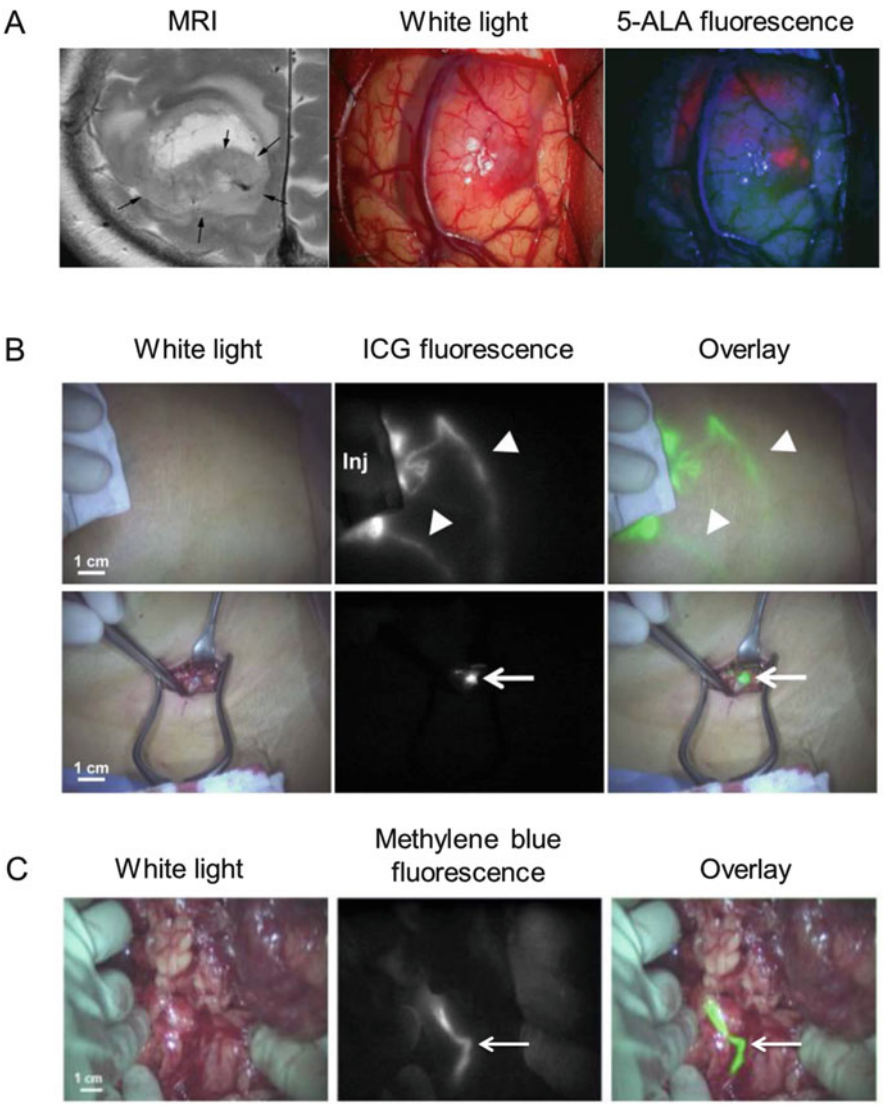


**Fig. 2** Examples of intraoperative imaging for detection and guidance of surgical intervention. (**a**) Images from a glioblastoma patient. Left, an MRI scan of the tumor following 5-ALA administration. Arrows indicate a part of the tumor showing increase of signal following 5-ALA administration. Center and right, intraoperative images showing tumor contrast of the frontal lobe under white light and violet-blue excitation fluorescence, respectively [42]. (**b**) NIR fluorescence imaging of lymph node biopsy from a breast cancer patient following ICG injection during percutaneous assessment (upper row) and in exposed sentinel lymph node (lower row). NIR fluorescence light penetrates tissue, allowing noninvasive imaging method of lymph nodes and lymphatic flow [43]. (**c**) NIR fluorescence imaging of the ureter during abdominal surgery following intravenous administration of methylene blue [44]. Referenced figure panels have been adapted and reprinted with permission of their respective owners

Targeted contrast agents for intraoperative imaging include amino acids and peptides such as aminolevulinic acid, cyclic arginine-glycine-aspartate (cRGD), folate, chlorotoxin, and specific antibodies against antigens such as CA19-9, carcinoembryonic antigen (CEA), epithelial cell adhesion molecule (EPCAM), PSMA, and epidermal growth factor receptor (EGFR) [28, 39]. In organic probes, the NIR fluorophores are usually conjugated to a specific targeting ligand or monoclonal antibody. NIR agents target biomarkers expressed on certain types of cancers. Antibodies for imaging increased expression of growth factor receptors such as EGFR, Her2/neu receptor, or vascular endothelial growth factor (VEGF) receptor are labeled with Cyanine 5.5 and Alexa Fluor 750 fluorophores. Fluorophores bound to a specific ligand, e.g., VEGF or EGF, can be internalized, allowing uptake of the tracer to be monitored [28].

For imaging tumor angiogenesis, alpha-v-beta-3 ($\alpha_v\beta_3$) integrin, a well-characterized adhesion molecule found at the sprouting ends of newly formed blood vessels, can easily be targeted with molecular probes. For this reason, it has been used to model targeting of agents to tumors. High expression of adhesion receptors can be detected when targeting $\alpha_v\beta_3$ integrin with cRGD conjugated to Cyanine 5.5 or IRdye800CW [28]. Previous studies demonstrated that integrin $\alpha_v\beta_3$ or CD13 molecules, overexpressed specifically on the surfaces of endothelial or tumor cells, can serve as imaging targets for early tumor detection and NIR fluorescence-guided surgical navigation in glioblastomas [49, 57, 58].

Similar approaches using activatable fluorophores are followed when targeting the upregulation of tumor-associated proteolytic enzymes such as cathepsins and matrix metalloproteinases (MMP). This allows detection of proteases abundant in malignant tissue, which can be associated with specific invasive, aggressive, or metastatic characteristics of tumors. However, proteolytic enzymes are not specific for molecules in cancer cells, because cathepsins and matrix metalloproteinases are abundant in inflammatory tissue. NIR probes activated by proteases such as Cathepsin B and MMP-2 were injected in an inactivated state (quenched), and cleaved by enzymes that result in dequenching and increased fluorescence [28, 59].

**Summary** Integration of optical imaging in intraoperative guidance is necessary to improve the surgical accuracy and outcomes of clinical cancer surgery.

## 4 Cerenkov Luminescence Imaging and Therapy

**Cerenkov Luminescence** Cerenkov luminescence (CL) or Cerenkov radiation is a continuous spectrum of light peaking in the blue-to-ultraviolet spectrum. It is produced by subatomic charged particles traveling faster than the speed of light through a dielectric medium such as water or biological tissues. CL was discovered in 1934, but it was first recognized for biomedical research applications in 2009 due to advances in highly sensitive optical cameras [60, 61]. Since then, the applications of CL from clinically relevant radionuclides have been expanding to biomedical

imaging as well as cancer imaging and therapy. Cerenkov luminescence imaging (CLI) is a new medical imaging modality that captures CL emitted from clinically relevant radionuclides via optical imaging instruments and allows multimodal imaging in combination with positron emission tomography (PET) imaging. Further, CL has been applied with nanomaterials, small molecules, and biomolecules for better imaging and therapy in cancer research. This section covers the basics of CL and the recent advances of CLI for diagnosis of disease as well as its applications to cancer therapies.

In 1934, the Russian scientist Pavel Alekseyevich Cerenkov observed faint blue light when he accidentally placed a sulfuric acid solution over radium salts [62]. He concluded the observed visible light was produced by charged subatomic particles traveling faster than the phase velocity of light in a dielectric medium [63]. Further theoretical studies were conducted by Ilya Frank and Igor Tamm, who described the significance of particle energy, cone angle of emitted light, and refractive index of media. In 1958, Cerenkov, Frank, and Tamm were awarded the Nobel Prize in Physics for their discovery and explanation of the Cerenkov effect.

Positrons and electrons, collectively referred to as charged beta (β) particles, are produced by radioactive decay. In dielectric media (mainly tissue/water in biomedical contexts), β particles are traveling faster than the phase velocity of light. Charged β particles with high energy interact with surrounding water and polarize the randomly oriented water molecules. The polarized water molecules then relax to the ground state by emitting photons in the direction of the charged particle travel, creating a coherent wavefront [61]. The photons propagate at a forward angle ($\theta$) from the direction of the charged particle vector.

**Cerenkov Luminescence Imaging** The Cerenkov phenomenon has been applied in the fields of physics and engineering in a variety of applications, such as in detectors for particle physics and nuclear power plants [64]. In 2009, the first biomedical imaging application of the Cerenkov phenomenon was reported by Robertson et al. who described Cerenkov luminescence imaging (CLI), using $^{18}$F-fluorodeoxyglucose ($^{18}$F-FDG) in vivo imaged with widely used optical instrumentation for bioluminescence imaging, which provides the necessary sensitivity [60]. This study set the foundation of CLI, and biomedical applications of CLI have been rapidly expanding ever since. CLI provides a quantitative multimodal imaging system in conjunction with positron emission tomography (PET) and could be advantageous over the conventional imaging modalities in the clinic in terms of cost, time, and applicability of radionuclides (Fig. 3a, b). Some preclinical studies for CLI have been reported using clinically relevant radionuclides including $^{18}$F, $^{89}$Zr, $^{90}$Y, $^{68}$Ga, and $^{225}$Ac [65, 67].

CLI for experimental imaging in small animals utilizes a bioluminescence imaging system equipped with a charged coupled device (CCD) camera in a chamber to exclude ambient light [68]. $^{18}$F-FDG, a radiotracer for glycolytic metabolism, is one of the most common radiotracers for PET imaging because it preferentially accumulates in cancer cells [69]. CL from $^{18}$F-FDG has been shown to strongly correlate with signal intensity in PET imaging [70]. In addition to small-molecule

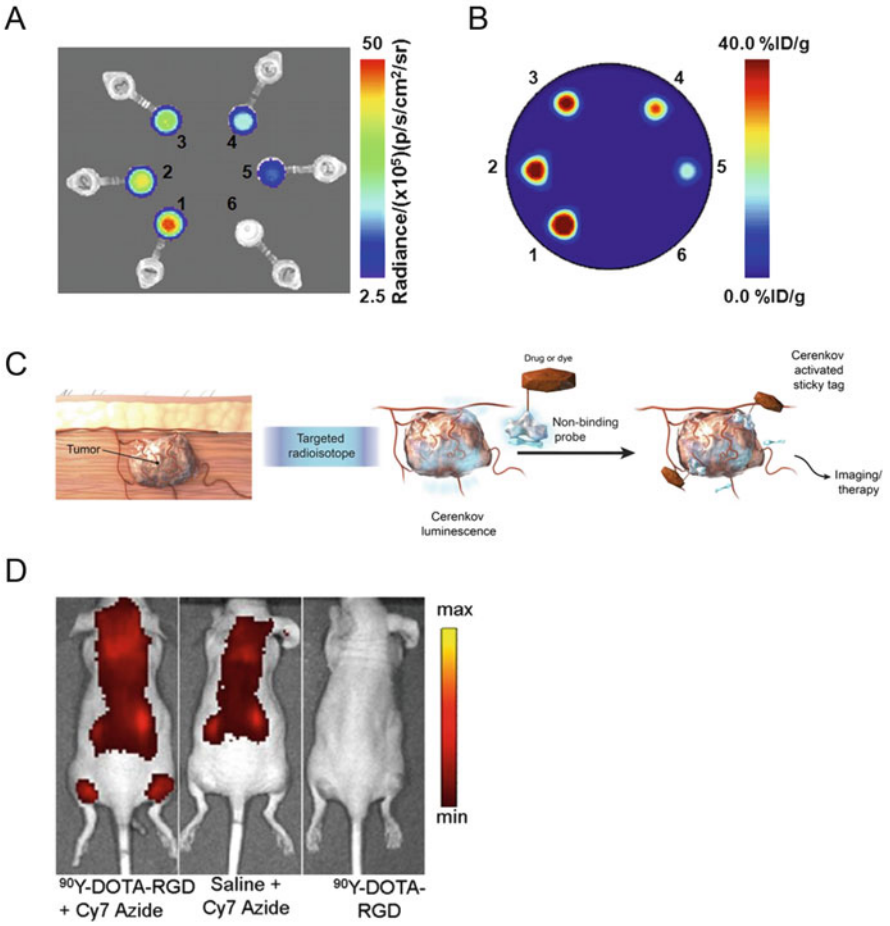


**Fig. 3** (**a**) Cerenkov luminescence imaging and (**b**) PET imaging of $^{89}$Zr in water. The activity concentrations of $^{89}$Zr decrease sequentially in samples 1–6, ranging from 40.3 kBq/mL in sample 1 to 0.0 kBq/mL in sample 6 [65]. (**c**) Schematic of CL-activated "sticky tag" technology [66]. (**d**) Fluorescence image of mice injected with Cyanine 7-azide following previous administration of the $\alpha_v\beta_3$-integrin-binding radiotracer $^{90}$Y-DOTA-RGD. Enrichment of Cyanine 7 signal can be observed in the $\alpha_v\beta_3$-integrin-expressing tumors on the left and right rear flanks due to activation of the azide group "sticky tag" by CL [66]. Referenced figure panels have been adapted and reprinted with permission of their respective owners

radiotracers, CLI with biomolecule radiotracers such as peptides and antibodies has also been reported. For example, a gastrin-releasing peptide receptor, or bombesin receptor, agonist was labeled with $^{90}$Y and enabled imaging of prostate tumors in mice by CLI [71]. Further, the anti-prostate-specific membrane antigen (PSMA) antibody labeled with $^{64}$Cu was shown to visualize PSMA-positive tumors in mice by both CLI and PET [72].

In addition to small molecules and biomolecules, CLI is also compatible with in vivo imaging of nanoparticles. Nanoparticles have gathered much attention in biomedical research because of their unique properties, including ease of preparations and modifications, and better pharmacological properties than some conventional chemotherapeutic agents. Some nanoparticles are excitable by Cerenkov light and emit in longer wavelengths. The imaging system utilizing this phenomenon is called synonymously secondary Cerenkov-induced fluorescence imaging (SCIFI) or Cerenkov radiation energy transfer (CRET). The higher optical cross section of certain nanoparticles sometimes permits SCIFI or CRET [61]. For example, quantum nanoparticles (Qtracker 705) and quantum dots (QD605) have been shown to be excited by CL to emit longer wavelengths of light, which is advantageous to overcome the poor tissue permeability of UV light [63, 73]. However, the system of SCIFI or CRET is not easily modulated because it can be activated regardless of the surrounding environment. Hence, smart activatable agents, which could be modulated by endogenous or exogenous stimuli when needed, may provide the basis of a more accurate imaging system. Photoactivation of caged luciferin by CL is one example of a smart activatable agent [74]. Luciferin is caged by an orthonitrobenzyl ether protecting group, which is known to be activated by UV light. CL from $^{18}$F-FDG successfully uncaged luciferin, the substrate of luciferase, and induced bioluminescence from cancer cells expressing luciferase. Another example of smart activatable agent is protease-activatable SCIFI, which can be turned on by matrix metallopeptidase-2 enzyme activity [75]. Fluorescein is tethered with a peptide to a gold nanoparticle and quenched due to the proximity of fluorescein and a gold nanoparticle; once the enzyme cleaves the peptide, the gold nanoparticle quencher is released and fluorescein becomes excitable by CL.

The major limitation of CLI is its low intensity of signal compared to conventional optical fluorescence imaging. The prolonged scanning time degrades image quality due to confounding factors such as patient movement, and the duration of imaging is limited because of the radionuclide half-life. The CL-activated "sticky tag" strategy may potentially overcome these limitations by translating CL into fluorescence (Fig. 3c) [76]. The sticky tag consists of a fluorescent dye tethered by an aryl azide group. UV light irradiation from Cerenkov transforms the azide into a singlet nitrene, which can be chemically incorporated into biomolecules on cellular plasma membranes or proteins in the intracellular matrix. Therefore, radioactivity, from, e.g., $^{18}$F-FDG or an $^{89}$Zr-labeled antibody, is converted to fluorescence that is attached to the side of the radioactive decay. The photoactivation of Cyanine 7-azide is demonstrated in both in vitro and in vivo (Fig. 3d).

The first human CLI was performed in 2013. CL with 550 MBq of $^{131}$I from the thyroid gland of a patient treated for hyperthyroidism was detected using an electron multiplied CCD camera [77]. In this study, photographic light and CL were successfully localized in the thyroid region. However, the first human study did not provide quantification of the thyroid. A more rigorous study was performed in the same year using $^{18}$F-FDG in lymphoma patients, lung cancer, and breast cancer [78]. Patients undergoing diagnostic $^{18}$F-FDG PET/CT scans were tested for the feasibility of CLI. A cooled CCD camera was used to monitor CL and quantification

was implemented. The study demonstrated the linear correlation between the activity of radionuclides and the intensity of CL and also showed that the diagnostic dose of $^{18}$F-FDG is feasible for detecting nodal disease by CLI.

**Cerenkov-Induced Therapy** The applications of CL have also been rapidly expanding to cancer therapy. Photodynamic therapy (PDT) utilizes photosensitizers, which absorb light and produce reactive oxygen species (ROS) to kill cancerous cells. Conventional PDT uses red-to-infrared light from external light sources to excite the photosensitizers. Because the tissue permeability of light is poor, the light source needs to be delivered to the deep tumor site by insertion of fiber optics into the patient's body. This invasive approach could be avoided by CL-induced PDT. Photosensitizers in proximity to clinically relevant radionuclides may be excitable by CL, resulting in localized cytotoxic ROS generation. It was demonstrated that CL generated by $^{90}$Y excites porphyrin, a photosensitizer, and inhibits cell growth [79]. Furthermore, nanoparticles have shown some promising results as a part of CL-based PDT strategies. For example, it was demonstrated that titanium dioxide could be excited by CL and generate ROS from water and oxygen molecules. Further, titanium dioxide in the presence of $^{18}$F-FDG or $^{64}$Cu could induce PDT in vivo [80]. In addition to titanium dioxide, some other nanoparticles have also been reported to induce PDT such as chlorin e6 nanoparticles and copper sulfide nanoparticles [81, 82].

**Summary** Cerenkov luminescence has garnered great attention in both science and medicine since the first biomedical application of CL was reported in 2009. CL provides an easy-to-prepare and cost-effective imaging modality. Because CL is generated by most PET imaging radiotracers, multimodal imaging with both CLI and PET may be possible. CL combined with small molecules, biomolecules, and nanoparticles has been studied to improve in vivo radiotracer tracking capabilities. Further, a new targeted therapeutic paradigm that selectively kills only cells in proximity to CL-generating radiotracers may be accomplished with CL. CL-induced PDT may provide a less invasive approach compared to the conventional PDT in the clinic. However, there are some limitations that must be overcome, such as the weak intensity of CL and prolonged exposure to high dose of radionuclides. Therefore, further development of this field is needed before clinical relevance can be achieved.

#### Compliance with Ethical Standards

**Conflict of Interest**: Evan P. Stater declares that he has no conflict of interest. Magdalena Skubal declares that she has no conflict of interest. Ryo Tamura declares that he has no conflict of interest. Jan Grimm declares that he has no conflict of interest.

**Ethical Approval**: This chapter does not contain any studies with human participants or animals performed by any of the authors.

**Funding**: Not applicable.

**Informed Consent**: Informed consent was obtained from all individual participants included in referenced studies.

## References


1. Capelle LG, Haringsma J, de Vries AC, Steyerberg EW, Biermann K, van Dekken H, Kuipers EJ (2010) Narrow band imaging for the detection of gastric intestinal metaplasia and dysplasia during surveillance endoscopy. Dig Dis Sci 55(12):3442–3448
2. Yoshida N, Naito Y, Inada Y, Kugai M, Inoue K, Uchiyama K, Handa O, Takagi T, Konishi H, Yagi N et al (2012) The detection of surface patterns by flexible spectral imaging color enhancement without magnification for diagnosis of colorectal polyps. Int J Color Dis 27 (5):605–611
3. Sato R, Fujiya M, Watari J, Ueno N, Moriichi K, Kashima S, Maeda S, Ando K, Kawabata H, Sugiyama R et al (2011) The diagnostic accuracy of high-resolution endoscopy, autofluorescence imaging and narrow-band imaging for differentially diagnosing colon adenoma. Endoscopy 43(10):862–868
4. Chang TC, Marcq G, Kiss B, Trivedi DR, Mach KE, Liao JC (2017) Image-guided transurethral resection of bladder tumors – current practice and future outlooks. Bladder Cancer 3 (3):149–159
5. Fu HL, Leng Y, Cobb MJ, Hsu K, Hwang JH, Li X (2008) Flexible miniature compound lens design for high-resolution optical coherence tomography balloon imaging catheter. J Biomed Opt 13(6):060502
6. Kang HS, Hong SN, Kim YS, Park HS, Kim BK, Lee JH, Kim SI, Lee TY, Kim JH, Lee SY et al (2013) The efficacy of i-SCAN for detecting reflux esophagitis: a prospective randomized controlled trial. Dis Esophagus 26(2):204–211
7. Li CQ, Li Y, Zuo XL, Ji R, Li Z, Gu XM, Yu T, Qi QQ, Zhou CJ, Li YQ (2013) Magnified and enhanced computed virtual chromoendoscopy in gastric neoplasia: a feasibility study. World J Gastroenterol 19(26):4221–4227
8. Basford PJ, Longcroft-Wheaton G, Higgins B, Bhandari P (2014) High-definition endoscopy with i-SCAN for evaluation of small colon polyps: the HiSCOPE study. Gastrointest Endosc 79(1):111–118
9. Osawa H, Yamamoto H, Miura Y, Ajibe H, Shinhata H, Yoshizawa M, Sunada K, Toma S, Satoh K, Sugano K (2012) Diagnosis of depressed-type early gastric cancer using small-caliber endoscopy with flexible spectral imaging color enhancement. Dig Endosc 24(4):231–236
10. Aminalai A, Rosch T, Aschenbeck J, Mayr M, Drossel R, Schroder A, Scheel M, Treytnar D, Gauger U, Stange G et al (2010) Live image processing does not increase adenoma detection rate during colonoscopy: a randomized comparison between FICE and conventional imaging (Berlin Colonoscopy Project 5, BECOP-5). Am J Gastroenterol 105(11):2383–2388
11. Kato M, Kaise M, Yonezawa J, Goda K, Toyoizumi H, Yoshimura N, Yoshida Y, Kawamura M, Tajiri H (2009) Trimodal imaging endoscopy may improve diagnostic accuracy of early gastric neoplasia: a feasibility study. Gastrointest Endosc 70(5):899–906
12. Barnes TG, Hompes R, Birks J, Mortensen NJ, Jones O, Lindsey I, Guy R, George B, Cunningham C, Yeung TM (2018) Methylene blue fluorescence of the ureter during colorectal surgery. Surg Endosc 32(9):4036–4043
13. Karstensen JG, Cartana T, Constantinescu C, Dumitrascu S, Kovacevic B, Klausen P, Hassan H, Klausen TW, Bertani H, Bhutani MS et al (2018) Endoscopic ultrasound guided needle-based confocal laser endomicroscopy in solid pancreatic masses – a prospective validation study. Endosc Int Open 6(1):E78–E85
14. Meining A, Chen YK, Pleskow D, Stevens P, Shah RJ, Chuttani R, Michalek J, Slivka A (2011) Direct visualization of indeterminate pancreaticobiliary strictures with probe-based confocal laser endomicroscopy: a multicenter experience. Gastrointest Endosc 74(5):961–968
15. Schmidbauer J, Remzi M, Klatte T, Waldert M, Mauermann J, Susani M, Marberger M (2009) Fluorescence cystoscopy with high-resolution optical coherence tomography imaging as an adjunct reduces false-positive findings in the diagnosis of urothelial carcinoma of the bladder. Eur Urol 56(6):914–919

16. Ding M, Chen Y, Guan WJ, Zhong CH, Jiang M, Luo WZ, Chen XB, Tang CL, Tang Y, Jian QM et al (2016) Measuring airway remodeling in patients with different COPD staging using endobronchial optical coherence tomography. Chest 150(6):1281–1290
17. Gora MJ, Simmons LH, Queneherve L, Grant CN, Carruth RW, Lu W, Tiernan A, Dong J, Walker-Corkery B, Soomro A et al (2016) Tethered capsule endomicroscopy: from bench to bedside at a primary care practice. J Biomed Opt 21(10):104001
18. Rotondano G, Bianco MA, Sansone S, Prisco A, Meucci C, Garofano ML, Cipolletta L (2012) Trimodal endoscopic imaging for the detection and differentiation of colorectal adenomas: a prospective single-centre clinical evaluation. Int J Color Dis 27(3):331–336
19. Bergholt MS, Lin K, Wang J, Zheng W, Xu H, Huang Q, Ren JL, Ho KY, Teh M, Srivastava S et al (2016) Simultaneous fingerprint and high-wavenumber fiber-optic Raman spectroscopy enhances real-time in vivo diagnosis of adenomatous polyps during colonoscopy. J Biophotonics 9(4):333–342
20. Wang J, Lin K, Zheng W, Ho KY, Teh M, Yeoh KG, Huang Z (2015) Comparative study of the endoscope-based bevelled and volume fiber-optic Raman probes for optical diagnosis of gastric dysplasia in vivo at endoscopy. Anal Bioanal Chem 407(27):8303–8310
21. Ming LC, Gangodu NR, Loh T, Zheng W, Wang J, Lin K, Zhiwei H (2017) Real time near-infrared Raman spectroscopy for the diagnosis of nasopharyngeal cancer. Oncotarget 8 (30):49443–49450
22. Kothapalli SR, Liu H, Liao JC, Cheng Z, Gambhir SS (2012) Endoscopic imaging of Cerenkov luminescence. Biomed Opt Express 3(6):1215–1225
23. Friedland S, Benaron D, Parachikov I, Soetikno R (2003) Measurement of mucosal capillary hemoglobin oxygen saturation in the colon by reflectance spectrophotometry. Gastrointest Endosc 57(4):492–497
24. Friedland S, Benaron D, Coogan S, Sze DY, Soetikno R (2007) Diagnosis of chronic mesenteric ischemia by visible light spectroscopy during endoscopy. Gastrointest Endosc 65(2):294–300
25. Meng G, Liang Y, Sarsfield S, Jiang WC, Lu R, Dudman JT, Aponte Y, Ji N (2019) High-throughput synapse-resolving two-photon fluorescence microendoscopy for deep-brain volumetric imaging in vivo. elife 8
26. Bocarsly ME, Jiang WC, Wang C, Dudman JT, Ji N, Aponte Y (2015) Minimally invasive microendoscopy system for in vivo functional imaging of deep nuclei in the mouse brain. Biomed Opt Express 6(11):4546–4556
27. Weissleder R, Pittet MJ (2008) Imaging in the era of molecular oncology. Nature 452 (7187):580–589
28. Keereweer S, Kerrebijn JD, van Driel PB, Xie B, Kaijzel EL, Snoeks TJ, Que I, Hutteman M, van der Vorst JR, Mieog JS et al (2011) Optical image-guided surgery – where do we stand? Mol Imaging Biol 13(2):199–207
29. Rosenthal EL, Warram JM, de Boer E, Basilion JP, Biel MA, Bogyo M, Bouvet M, Brigman BE, Colson YL, DeMeester SR et al (2016) Successful translation of fluorescence navigation during oncologic surgery: a consensus report. J Nucl Med 57(1):144–150
30. Mondal SB, Gao S, Zhu N, Liang R, Gruev V, Achilefu S (2014) Real-time fluorescence image-guided oncologic surgery. Adv Cancer Res 124:171–211
31. Haque R, Contreras R, McNicoll MP, Eckberg EC, Petitti DB (2006) Surgical margins and survival after head and neck cancer surgery. BMC Ear Nose Throat Disord 6:2
32. Eldeeb H, Macmillan C, Elwell C, Hammod A (2012) The effect of the surgical margins on the outcome of patients with head and neck squamous cell carcinoma: single institution experience. Cancer Biol Med 9(1):29–33
33. Pirro V, Alfaro CM, Jarmusch AK, Hattab EM, Cohen-Gadol AA, Cooks RG (2017) Intraoperative assessment of tumor margins during glioma resection by desorption electrospray ionization-mass spectrometry. Proc Natl Acad Sci U S A 114(26):6700–6705
34. Sawabata N, Ohta M, Matsumura A, Nakagawa K, Hirano H, Maeda H, Matsuda H, Thoracic Surgery Study Group of Osaka U (2004) Optimal distance of malignant negative margin in excision of nonsmall cell lung cancer: a multicenter prospective study. Ann Thorac Surg 77 (2):415–420

35. Nagtegaal ID, Quirke P (2008) What is the role for the circumferential margin in the modern treatment of rectal cancer? J Clin Oncol 26(2):303–312
36. Dotan ZA, Kavanagh K, Yossepowitch O, Kaag M, Olgac S, Donat M, Herr HW (2007) Positive surgical margins in soft tissue following radical cystectomy for bladder cancer and cancer specific survival. J Urol 178(6):2308–2312. discussion 2313
37. Reyna C, DeSnyder SM (2018) Intraoperative margin assessment in breast cancer management. Surg Oncol Clin N Am 27(1):155–165
38. Hong X, Li T, Ling F, Yang D, Hou L, Li F, Tan W (2017) Impact of surgical margin status on the outcome of bladder cancer treated by radical cystectomy: a meta-analysis. Oncotarget 8 (10):17258–17269
39. Nguyen QT, Tsien RY (2013) Fluorescence-guided surgery with live molecular navigation – a new cutting edge. Nat Rev Cancer 13(9):653–662
40. Wang C, Wang Z, Zhao T, Li Y, Huang G, Sumer BD, Gao J (2018) Optical molecular imaging for tumor detection and image-guided surgery. Biomaterials 157:62–75
41. Hiroshima Y, Maawy A, Metildi CA, Zhang Y, Uehara F, Miwa S, Yano S, Sato S, Murakami T, Momiyama M et al (2014) Successful fluorescence-guided surgery on human colon cancer patient-derived orthotopic xenograft mouse models using a fluorophore-conjugated anti-CEA antibody and a portable imaging system. J Laparoendosc Adv Surg Tech A 24(4):241–247
42. Yamamoto J, Kakeda S, Yoneda T, Ogura SI, Shimajiri S, Tanaka T, Korogi Y, Nishizawa S (2017) Improving contrast enhancement in magnetic resonance imaging using 5-aminolevulinic acid-induced protoporphyrin IX for high-grade gliomas. Oncol Lett 13(3):1269–1275
43. Schaafsma BE, Mieog JS, Hutteman M, van der Vorst JR, Kuppen PJ, Lowik CW, Frangioni JV, van de Velde CJ, Vahrmeijer AL (2011) The clinical use of indocyanine green as a near-infrared fluorescent contrast agent for image-guided oncologic surgery. J Surg Oncol 104 (3):323–332
44. Verbeek FP, van der Vorst JR, Schaafsma BE, Swijnenburg RJ, Gaarenstroom KN, Elzevier HW, van de Velde CJ, Frangioni JV, Vahrmeijer AL (2013) Intraoperative near infrared fluorescence guided identification of the ureters using low dose methylene blue: a first in human experience. J Urol 190(2):574–579
45. Stummer W, Novotny A, Stepp H, Goetz C, Bise K, Reulen HJ (2000) Fluorescence-guided resection of glioblastoma multiforme by using 5-aminolevulinic acid-induced porphyrins: a prospective study in 52 consecutive patients. J Neurosurg 93(6):1003–1013
46. Stummer W, Pichlmeier U, Meinel T, Wiestler OD, Zanella F, Reulen HJ, Group AL-GS (2006) Fluorescence-guided surgery with 5-aminolevulinic acid for resection of malignant glioma: a randomised controlled multicentre phase III trial. Lancet Oncol 7(5):392–401
47. Shou K, Qu C, Sun Y, Chen H, Chen S, Zhang L, Xu H, Hong X, Yu A, Cheng Z (2017) Multifunctional biomedical imaging in physiological and pathological conditions using a NIR-II probe. Adv Funct Mater 27(23):1700995
48. Antaris AL, Chen H, Cheng K, Sun Y, Hong G, Qu C, Diao S, Deng Z, Hu X, Zhang B et al (2016) A small-molecule dye for NIR-II imaging. Nat Mater 15(2):235–242
49. Liu Y, Wang Z, Li X, Ma X, Wang S, Kang F, Yang W, Ma W, Wang J (2019) Near-infrared fluorescent peptides with high tumor selectivity: novel probes for image-guided surgical resection of orthotopic glioma. Mol Pharm 16:108–117
50. Vahrmeijer AL, Hutteman M, van der Vorst JR, van de Velde CJ, Frangioni JV (2013) Image-guided cancer surgery using near-infrared fluorescence. Nat Rev Clin Oncol 10(9):507–518
51. van der Poel HG, Buckle T, Brouwer OR, Valdes Olmos RA, van Leeuwen FW (2011) Intraoperative laparoscopic fluorescence guidance to the sentinel lymph node in prostate cancer patients: clinical proof of concept of an integrated functional imaging approach using a multimodal tracer. Eur Urol 60(4):826–833
52. Mieog JS, Troyan SL, Hutteman M, Donohoe KJ, van der Vorst JR, Stockdale A, Liefers GJ, Choi HS, Gibbs-Strauss SL, Putter H et al (2011) Toward optimization of imaging system and lymphatic tracer for near-infrared fluorescent sentinel lymph node mapping in breast cancer. Ann Surg Oncol 18(9):2483–2491

53. Vuijk FA, Hilling DE, Mieog JSD, Vahrmeijer AL (2018) Fluorescent-guided surgery for sentinel lymph node detection in gastric cancer and carcinoembryonic antigen targeted fluorescent-guided surgery in colorectal and pancreatic cancer. J Surg Oncol 118(2):315–323
54. Handgraaf HJ, Boogerd LS, Verbeek FP, Tummers QR, Hardwick JC, Baeten CI, Frangioni JV, van de Velde CJ, Vahrmeijer AL (2016) Intraoperative fluorescence imaging to localize tumors and sentinel lymph nodes in rectal cancer. Minim Invasive Ther Allied Technol 25(1):48–53
55. Verbeek FP, Tummers QR, Rietbergen DD, Peters AA, Schaafsma BE, van de Velde CJ, Frangioni JV, van Leeuwen FW, Gaarenstroom KN, Vahrmeijer AL (2015) Sentinel lymph node biopsy in vulvar cancer using combined radioactive and fluorescence guidance. Int J Gynecol Cancer 25(6):1086–1093
56. van Leeuwen FWB, Winter A, van Der Poel HG, Eiber M, Suardi N, Graefen M, Wawroschek F, Maurer T (2019) Technologies for image-guided surgery for managing lymphatic metastases in prostate cancer. Nat Rev Urol 16:159–171
57. Jain RK, Duda DG, Willett CG, Sahani DV, Zhu AX, Loeffler JS, Batchelor TT, Sorensen AG (2009) Biomarkers of response and resistance to antiangiogenic therapy. Nat Rev Clin Oncol 6 (6):327–338
58. Ribatti D, Ranieri G, Basile A, Azzariti A, Paradiso A, Vacca A (2012) Tumor endothelial markers as a target in cancer. Expert Opin Ther Targets 16(12):1215–1225
59. Mahmood U, Weissleder R (2003) Near-infrared optical imaging of proteases in cancer. Mol Cancer Ther 2(5):489–496
60. Robertson R (2009) Optical imaging of Cerenkov light generation from positron-emitting radiotracers. Phys Med Biol 54:N355–N365
61. Shaffer TM, Pratt EC, Grimm J (2017) Utilizing the power of Cerenkov light with nanotechnology. Nat Nanotechnol 12:106–117
62. Bolotovskii BM (2009) Vavilov – Cherenkov radiation: its discovery and application. Physics-Uspekhi 52:1099–1110
63. Das S, Thorek DLJ, Grimm J (2014) Cerenkov imaging. Adv Cancer Res 124:213–234
64. Thorek DLJ, Robertson R, Bacchus WA, Hahn J, Rothberg J, Beattie BJ, Grimm J (2012) Cerenkov imaging – a new modality for molecular imaging. Am J Nucl Med Mol Imaging 2:163–173
65. Ruggiero A, Holland JP, Lewis JS, Grimm J (2010) Cerenkov luminescence imaging of medical isotopes. J Nucl Med 51:1123–1130
66. Das S, Haedicke K, Grimm J (2018) Cerenkov-activated sticky tag for in vivo fluorescence imaging. J Nucl Med 59(1):58–65
67. Pratt EC, Shaffer TM, Grimm J (2016) Nanoparticles and radiotracers: advances toward radionanomedicine. WIREs Nanomed Nanobiotechnol 8:872–890
68. Tamura R, Pratt EC, Grimm J (2018) Innovations in nuclear imaging instrumentation: Cerenkov imaging. Semin Nucl Med 48:359–366
69. Calvaresi EC, Hergenrother PJ (2013) Glucose conjugation for the specific targeting and treatment of cancer. Chem Sci 4:2319–2333
70. Liu H, Ren G, Miao Z, Zhang X, Tang X, Han P, Sanjiv S (2010) Molecular optical imaging with radioactive probes. PLoS One 5:e9470
71. Lohrmann C, Zhang H, Thorek DLJ, Desai P, Zanzonico PB, O'Donoghue J, Irwin CP, Reiner T, Grimm J, Weber WA (2015) Cerenkov luminescence imaging for radiation dose calculation of a 90y-labeled gastrin-releasing peptide receptor antagonist. J Nucl Med 56 (5):805–811
72. D'Souza JW, Hensley H, Doss M, Beigarten C, Torgov M, Olafsen T, Yu JQ, Robinson MK (2017) Cerenkov luminescence imaging as a modality to evaluate antibody-based pet radiotracers. J Nucl Med 58(1):175–180
73. Dothager RS, Goiffon RJ, Jackson E, Harpstrite S, Piwnica-Worms D (2010) Cerenkov radiation energy transfer (CRET) imaging: a novel method for optical imaging of pet isotopes in biological systems. PLoS One 5(10):e13300

74. Ran C, Zhang Z, Hooker J, Moore A (2012) In vivo photoactivation without "light": use of Cherenkov radiation to overcome the penetration limit of light. Mol Imaging Biol 14:156–162
75. Thorek DLJ, Ogirala A, Beattie BJ, Grimm J (2013) Quantitative imaging of disease signatures through radioactive decay signal conversion. Nat Med 19:1345–1350
76. Das S, Haedicke K, Grimm J (2017) Cerenkov-activated sticky tag for in vivo fluorescence imaging. J Nucl Med 117:198549
77. Spinelli AE, Ferdeghini M, Cavedon C, Zivelonghi E, Calandrino R, Fenzi A, Sbarbati A, Boschi F (2013) First human Cerenkography. J Biomed Opt 18(2):20502
78. Thorek DL, Riedl CC, Grimm J (2014) Clinical Cerenkov luminescence imaging of (18)F-FDG. J Nucl Med 55:95–98
79. Hartl BA, Hirschberg H, Marcu L, Cherry SR, Clinic M (2016) Radiation generated from yttrium-90. J Environ Pathol Toxicol Oncol 35:185–192
80. Kotagiri N, Cooper ML, Rettig M, Egbulefu C, Prior J, Cui G, Karmakar P, Zhou M, Yang X, Sudlow G et al (2018) Radionuclides transform chemotherapeutics into phototherapeutics for precise treatment of disseminated cancer. Nat Commun 9:275
81. Kamkaew A, Cheng L, Goel S, Valdovinos HF, Barnhart TE, Liu Z, Cai W (2016) Cerenkov radiation induced photodynamic therapy using chlorin e6-loaded hollow mesoporous silica nanoparticles. ACS Appl Mater Interfaces 8(40):26630–26637
82. Goel S, Ferreira CA, Chen F, Ellison PA, Siamof CM, Barnhart TE, Cai W (2018) Activatable hybrid nanotheranostics for tetramodal imaging and synergistic photothermal/photodynamic therapy. Adv Mater 30:1–9